Mineralogy of the Vicenice octahedrite

Mineralogie vícenického oktaedritu

(34 figs-text, 10 tabs)

ROMAN SKÁLA[1] – JIŘÍ FRÝDA[1] – JOSEF SEKANINA[†]

[1] *Czech Geological Survey, Klárov 3/131, 118 21 Praha 1; e-mail addresses: skala@cgu.cz and fryda@cgu.cz*

The iron meteorite Vicenice was recovered in October 1911 E of village Vícenice. Its original dimensions were 180 × 90 × 65 mm and weight 4650 g. Based on the bandwidth of kamacite lamellae the Vicenice iron is a medium octahedrite (Om). Chemically, this meteorite belongs to IID irons. Except kamacite and taenite, the meteorite also contains schreibersite, troilite, daubréelite, chromite and an unidentified chlorine-containing iron (hydro?)oxide. Schreibersite is encountered in several forms with distinct chemistries; one of them represents a Ni-dominant phase, which has been approved recently as a new mineral - nickelphosphide. Several troilite grains are characterized by elevated contents of chromium. Optical observations indicate that several shock-induced deformations affected the meteorite in the space. Cooling rate was estimated to be in the order of 1.5–2 °C/Ma. X-ray powder diffraction proved goethite and lepidocrocite as main corrosion products in the weathering crust coating the meteorite.

Key words: Vicenice octahedrite, mineralogy, schreibersite, nickelphosphide, troilite, daubréelite, chromite

History and description

The iron meteorite Vicenice was originally recovered in October 1911 about 400 m E of village Vícenice*, about 2 km SW of Náměšť nad Oslavou in Moravia. Figure 1 shows a detailed map of the village Vícenice and surrounding area, including the location of the find on the parcel # 344 marked with a dot. On this place, called locally "Velké Štěpky", the owner at the time, Mr. Jan Svoboda and his son-in-law worked a loam pit to manufacture bricks for barn construction. In the depth of about 3/4 m, they found a rather heavy, slightly elongated nodule with rusty surface. The exotic object attracted the attention of the finders and they deposited it in the house of one of them in the village. For a long time, the meteorite has been stored in a granary and occasionally also used as a weight when beeswax was pressed. Only after 50 years in 1961, relatives of one of original finders brought the meteorite to Professor Josef Sekanina of Purkyně's University in Brno for closer examination. Sekanina made an extensive optical and metallographic study and confirmed the extraterrestrial origin of the object beyond reasonable doubt. He also identified its major mineral components: kamacite, taenite, plessite, schreibersite, and troilite (Sekanina 1971a, b).

When brought for examination, a discontinuous layer of gray wax covered the meteorite, giving it a curious gray color and waxy luster. After this layer was removed the meteorite color was dark brown. The surface was irregular, with up to 8 mm thick layered crust of iron oxyhydroxides. Dimensions of the iron meteorite were 180 × 90 × 65 mm and weight was 4650 g. At one end, the meteorite was flattened whereas other parts were more or less rounded – the inner deformations found at the flattened end of the meteorite permits speculation that a part of the meteorite had been broken away along this plane. Original shape of the meteorite is obvious from photographs in Fig. 2.

Three slabs with thickness of 10, 20 and 3 mm, respectively, have been cut from the meteorite and then polished and/or etched and investigated optically. Their orientation is shown in Fig. 3; individual cuts are labeled

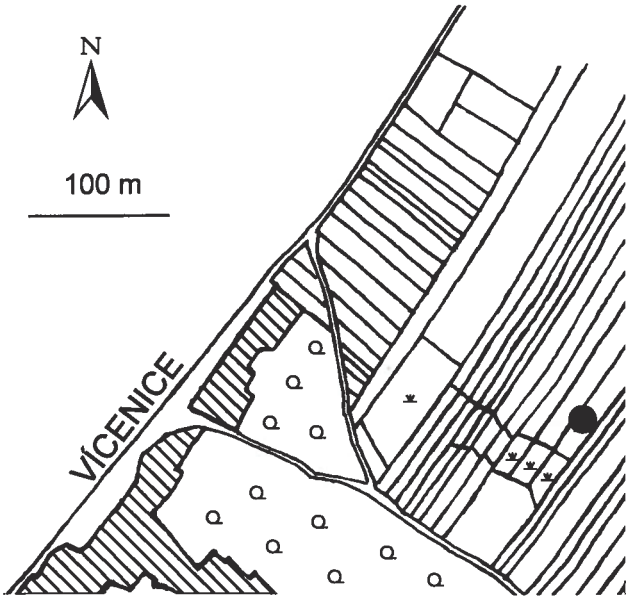

Fig. 1. Detailed map of the village Vícenice and the surrounding area, including the location of the meteorite recovery marked with a dot, on the parcel no. 344.

[†] Deceased on November 28, 1986. Because of his extensive contribution to the initial description of this meteorite, which, unfortunately, has never been published in English and adequately recognized, we include Professor Sekanina as a co-author of this paper, which contains many of his original data and photographs.

* Although the correct name of the village, after which the meteorite is named is 'Vícenice' this meteorite is listed as 'Vicenice' in all internationally recognized catalogues. Therefore, we use the latter spelling throughout this paper to be consistent with internationally accepted term.

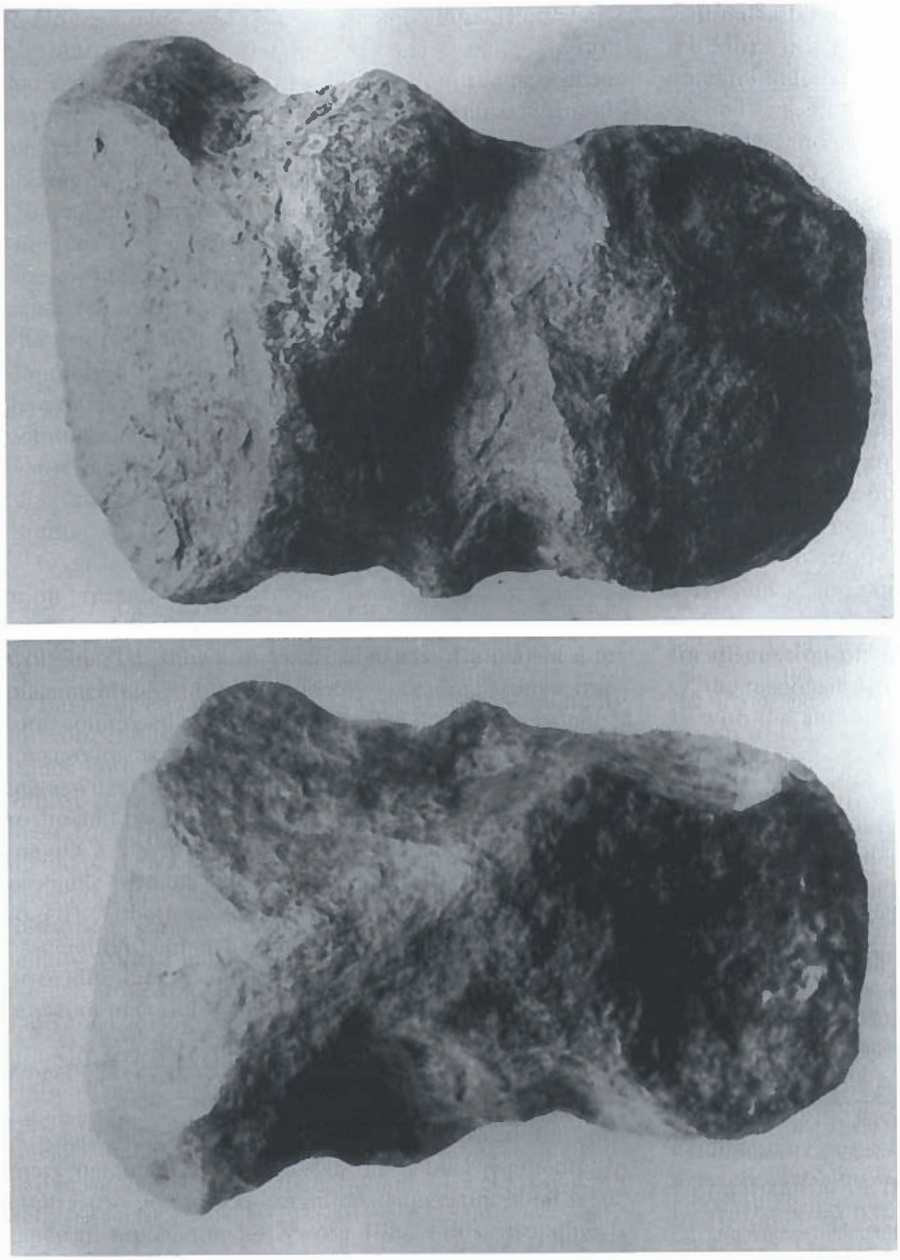

Fig. 2. The original shape of the Vicenice octahedrite. Note the flattened part along a part of the meteorite was probably broken away. The original dimensions were 180 × 90 × 65 mm and the weight was 4650 g.

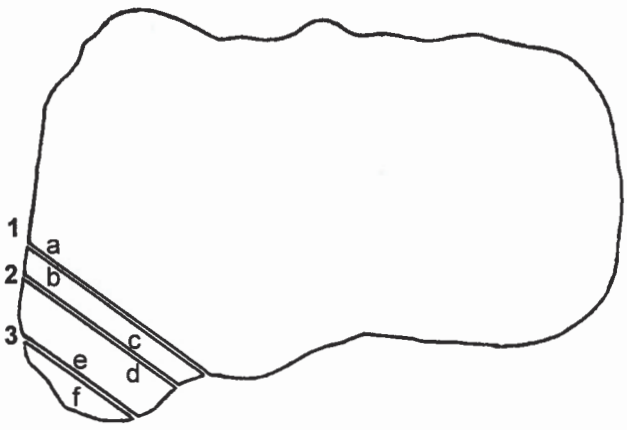

Fig. 3. Orientation of three parallel cuts (1 to 3) dividing the meteorite into 3 slices and a mainpiece. Letters 'a' to 'f' refer to the individual surfaces investigated. Wet chemical and INAA analyses were carried out on material sampled from surface 'b'. The surface labeled 'e' was used for acquisition of microprobe data.

1 to 3 whereas surfaces of the slices are labeled 'a' to 'f'. The surface labeled 'b' was used for sampling for wet chemical analysis, the results of which are given in Table 1. Today, the mainpiece of 3920 g in weight is deposited in the collections of the Moravian Museum in Brno, whereas the three slices (of 190 g, 87.5 g and 35 g weights) are in the meteorite collection of the Department of Mineralogy and Petrology of the National Museum in Prague (under catalogue # P1M 448, 449, and 450).

Classification

Based on the mean bandwidth of kamacite lamellae corrected for their 3D orientation, which is 0.63 mm, the Vicenice iron meteorite belongs to the group of medium octahedrites (Om). According to its minor and trace element composition (Table 2) the meteorite is classified as IID-iron (Wasson et al. 1989).

Table 1. Bulk chemical composition of the Vicenice meteorite according to the wet analysis by Dr. Pavel Povondra.

Fe	88.94
Ni	9.72
Co	0.63
P	0.272
S	0.008
Zn	0.083
Mg	0.024
Ca	0.195
SiO_2	0.087
Total	99.959

Table 2. Trace-element contents of the Vicenice meteorite, determined by INAA (Wasson et al. 1989).

Ni	(mg/g)	97.7	Sb	(μg/g)	0.11
Co	(mg/g)	6.8	W	(μg/g)	2.84
Cr	(μg/g)	47	Re	(μg/g)	1.22
Cu	(μg/g)	280	Ir	(μg/g)	12.7
Ga	(μg/g)	74.8	Pt	(μg/g)	16.1
Ge	(μg/g)	87.4	Au	(μg/g)	0.77
As	(μg/g)	6.68			

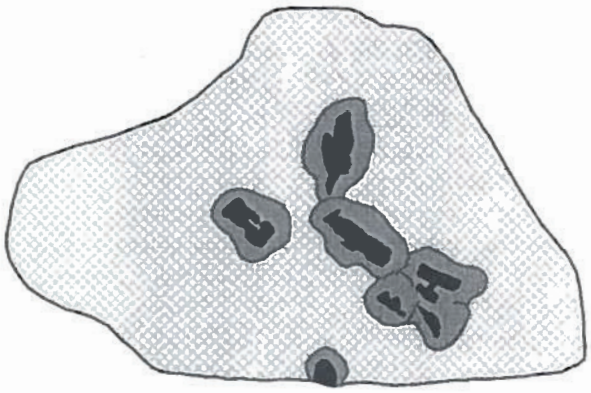

Fig. 4. Sketch of the surface 'e' examined by electron microprobe. Large skeletal aggregates of schreibersite are in black, swathing kamacite is dark gray.

Mineralogy

All available slices were studied optically by Sekanina. One polished carbon-coated slice of the meteorite (surface 'e' generated by cut #3 in Fig. 3, as schematized in Fig. 4) was investigated chemically using an energy-dispersive system Link eXL connected to a scanning electron microscope CamScan 4 by Skála and Frýda. Accelerating voltage was 20 kV and sample current 3 nA. Spectrum acquisition time was 80 s. Collected spectra were processed by the Link analytical software, which utilizes the correction procedure ZAF 4. Kamacite, taenite, troilite, and schreibersite were analyzed for Fe, Ni, Co, Cr, P, and S. Daubréelite and chromite were also analyzed for Zn, Mn, Mg and Ti. The standards used for elements quantification in metallic phases and sulfides were pure Ni, Fe, Co, and Zn, synthetic Fe_3P and pyrite (FeS_2). Synthetic olivines (Mg_2SiO_4, Fe_2SiO_4, Ni_2SiO_4, Mn_2SiO_4), corundum, quartz, chromite, synthetic TiO, and metallic Zn were utilized for chromite analyses. Normalization procedures leading to empirical formulae are given in each table, which summarizes analytical results in wt. % and atoms per formula unit (apfu).

Kamacite

Kamacite occurs in three different principal types: 1) coarse bands separated from each other by thin taenite lamellae, composing collectively the Widmanstätten pattern; 2) comb-, finger-, and flame-like bands in taenite matrix, forming the coarse-grained plessites; and 3) microscopically fine-grained, myrmekitic, micrographic, eutectoidal exsolutions in fine-grained plessites. Numerous gradual transitions between types 1 and 2 were also observed. Rarely, kamacite was also found as inclusions in euhedral to subhedral chromite crystals.

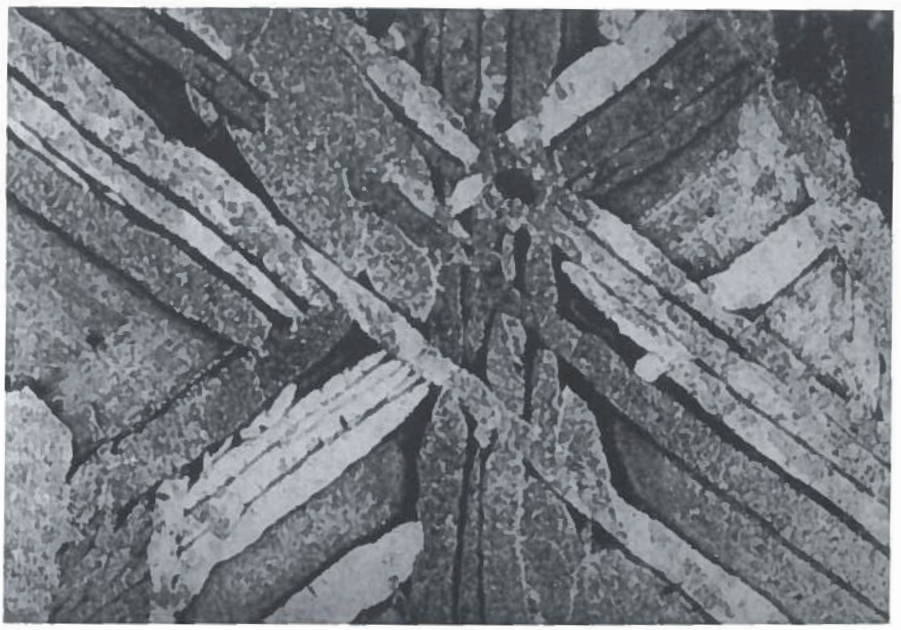

Fig. 5. Widmanstätten pattern on the surface 'a'. Note granulation in several kamacite bands and an oriented sheen. Directions of the three kamacite plate systems of the 1st generation are prominent and well evident, whereas orientation of broader plates of the fourth system is hard to follow. Along the edge of the section, there is a well-developed heat-affected zone generated by heating during the atmospheric entry and deceleration. Deeply etched. Longer side of the photograph equals 20 mm.

Fig. 6. Broad kamacite band of the fourth system with characteristic lobate outline. Note partial granulation. Etched. Longer side of the photograph equals 7.5 mm.

Bands of kamacite of the 1st type crisscross mutually in 4 directions. Three of these directions are dominant. Bands corresponding to these three orientations are of almost constant thickness (usually about 0.4–1.0 mm; mean bandwidth of kamacite lamellae is 0.63 mm). They maintain their orientations over the entire slice surface, indicating that the Vicenice octahedrite consisted originally of a single crystal of the γ-phase (Fig. 5). The length of these bands attains typically 2 cm, but several bands can be tracked over a distance of 3 cm. The L/W ratio for kamacite bands varies from 12 to 19. Longitudinal margins of bands are not perfectly straight but somewhat undulating. The bands pinch down at mutual intersections, which is characteristic of exsolution structures. The three dominant orientations of kamacite bands define angles 50 ± 1°, 56 ± 1°, and 74 ± 1°. Bands of the 4th direction (Fig. 6) are approximately 3 times broader (up to 2.5 mm). They have lobate outlines and their orientation can be estimated only with difficulty, because their overall elongation is not so pronounced as in the preceding three systems. Generally, their orientations dissect the above-mentioned angle of 56 ± 1°, generating a pair of angles ranging from 28° + 28° to 20° + 36° with mean angular values of 25° and 31°. Therefore, in the slices of the Vicenice octahedrite, the four systems of kamacite bands define angles 25°, 31°, 50°, and 74° in clockwise direction. It should be possible to determine from these angles the crystallographic orientation of the section planes with respect to octahedral planes. However, neither the use of Buchwald's (1969) tables nor the cyclographic projection lead to positive determination of crystallographic orientation of the cutting planes. This

Fig. 7. Swathing kamacite, up to 2 mm thick, along skeletal crystal of schreibersite (black). Etched. Longer side of the photograph equals 10 mm.

fact indicates that some kind of homogeneous deformation, due to uniaxial strain, most probably affected the planes defining the Widmanstätten pattern.

In the Vicenice meteorite, swathing kamacite enveloping larger schreibersite grains is also developed in a characteristic form. Its rounded outline more or less copies the shape of schreibersite cores (Figs 4 and 7). The thickness of these swathing kamacite rims is rather constant, ranging from 1.5 to 2 mm. Swathing kamacite nucleated before kamacite planes forming the Widmanstätten pattern started to grow, when atomic diffusion dominated and kamacite growth was at its fastest. This is documented by different crystallographic orientation of swathing kamacite from that of adjacent kamacite bands of the Widmanstätten pattern, which is evident from oriented-sheen observations on etched polished sections. Locally, swathing kamacite even continued to grow in this different orientation at the expense of neighboring kamacite bands after the Widmanstätten pattern had formed.

When observing oriented sheen on the etched meteorite slices and on the cut surface of the mainpiece it is evident that a mosaic of individual grains forms some kamacite bands and portions of swathing kamacite. This granulation is well developed for example in kamacite band of the 4th direction of the 1st type in Fig. 6. Present crystallographic orientation of these grains does not correspond to that of original Widmanstätten structure, indicating that deformation took place after kamacite had crystallized.

Taenite

Taenite forms thin lamellae, typically about 0.1 mm wide, intercalating kamacite bands. These taenite lamellae thin down where they are densely spaced and their nucleation planes were closer. These are the loci of the highest nickel content observed in taenite. In triangular or polygonal fields of kamacite bands, taenite forms rims of uniform thickness around kamacite; in contrast, in the inner parts of such fields taenite transforms to various types of plessite.

Plessite

Plessite – a mixture of kamacite and taenite lamellae of various thicknesses – is present in the Vicenice octahedrite, as in other octahedrites, in larger fields among kamacite bands where original taenite has been transformed due to later chemical differentiation.

The coarse-grained plessites resemble system of kamacite bands of the 1st type but at the smaller scale. The main difference is that lamellae of different orientations do not cross each other. Either the entire plessitic field is formed by a single system of parallel kamacite lamellae, or it is subdivided into individual sectors, each with a particular single orientation of kamacite bands of the 2nd type. Morphological features of kamacite lamellae of the 2nd generation are identical to those of kamacite bands of the 1st type. Three systems have narrower lamellae of comb-, finger-, or flame-like form, which thin down toward the boundary of the plessitic field. Kamacite lamellae of the fourth system are thicker and lobate. When sectioned subparallel to their platy shape, kamacite lamellae have an unevenly lobate shape (Fig. 8).

Out of various subtypes of coarse-grained plessites known in the literature, we can observe chiefly comb plessite in the Vicenice iron (Figs 9–10); other types of coarse plessites are either absent or only poorly developed here.

The fine-grained plessite consists of a microscopic mixture of kamacite and taenite, which is resolved only under high magnification. It occupies the inner parts of plessitic fields and coarsens towards the center of these fields, forming there an aggregate of fine-grained to acicular kamacite grains in taenite matrix. Locally, kamacite and taenite grains are intergrown in a myrmekitic aggregate. Also, in some parts of these fine-grained plessites, martensitic structure developed, modified by later recrystallization (Fig. 11). When completely evolved, the fine-grained plessite field is zoned: coarser-grained core of the plessitic field gradually changes to peripheral acicular rim whose needles intrude into extremely fine-grained, locally symplectitic, plessite. This fine-grained plessite further changes to a zone of taenite enriched in iron which slightly darkens on etching. Near the edge of the plessite field, there is a zone extremely enriched in nickel, with a steep Ni gradient and the maximum Ni content at the contact with kamacite band of the 1st type (Fig. 12).

Fine-grained plessites are represented in the Vicenice octahedrite chiefly by net plessite (Fig. 13). However, various types transitional to black plessite or black taenite were observed (Fig. 14).

Several plessite types are commonly present in a single plessitic field. Fine-grained plessites usually fill in spaces among kamacite bands of the 2nd generation, forming comb plessites. Distinct differences between the comb and net plessites, without any gradual transitions, indicate that they formed under different conditions.

The variability in composition of metallic phases is shown in Fig. 15 where concentrations in wt. % of nickel and cobalt are plotted against iron content. The plot indicates that kamacite contains typically between 5.3 to 7.3 wt. % Ni while taenite composition varies in a broad range up to 42 wt. % Ni. Characteristic M-profile traversing a single taenite lamella bound by kamacite bands is shown in Fig. 16. At the boundary, the nickel content attains ca 42 wt. %, at the center of the taenite lamella it is about 30 wt. %, whereas in adjacent kamacite the nickel content decreases to as low as ca 3 wt. %. Iron and cobalt contents have opposite trends.

Schreibersite

Schreibersite is the third most prominent mineral in the Vicenice octahedrite. Relatively large grains of schreibersite (up to 1 cm across), isometric to lath-shaped or skel-

Fig. 8. Comb plessite consisting of finger-shaped kamacite bands of the 2nd generation, crosscut in two different directions. Etched. Longer side of the photograph equals 0.36 mm.

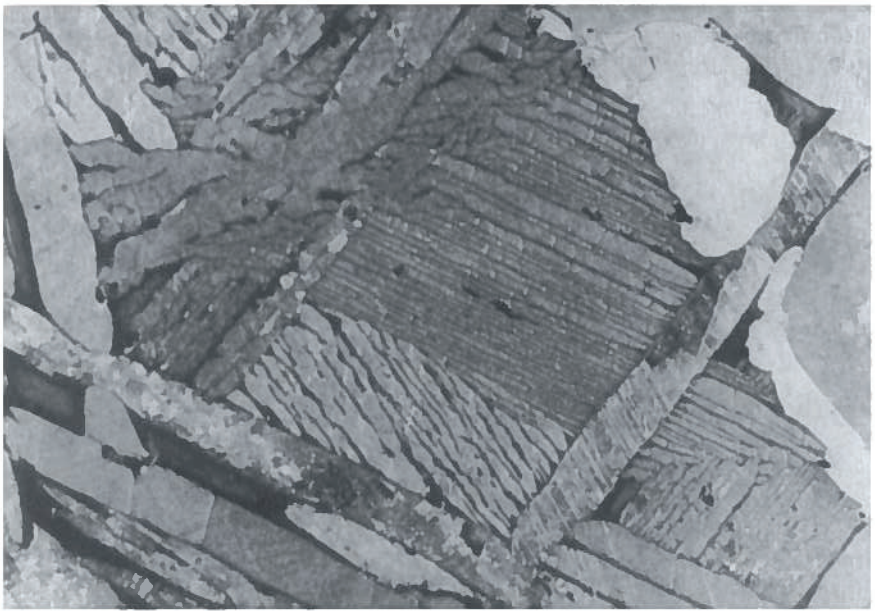

Fig. 9. Comb plessite. Note that kamacite bands in the plessite field do not cross each other, whereas those building up the Widmanstätten pattern do. Etched. Longer side of the photograph equals 7.5 mm.

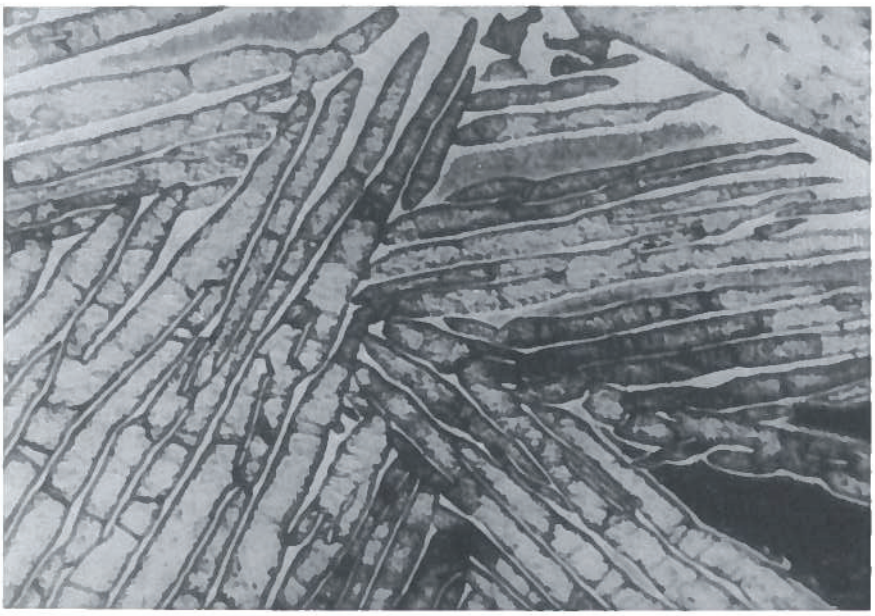

Fig. 10. Comb plessite formed by needle-shaped kamacite bands of the 2nd generation narrowing down to the contact with kamacite band of the 1st generation. Spaces among kamacite plates of the 2nd generation building up the plessite are filled in by taenite and black taenite. Etched. Longer side of the photograph equals 0.36 mm.

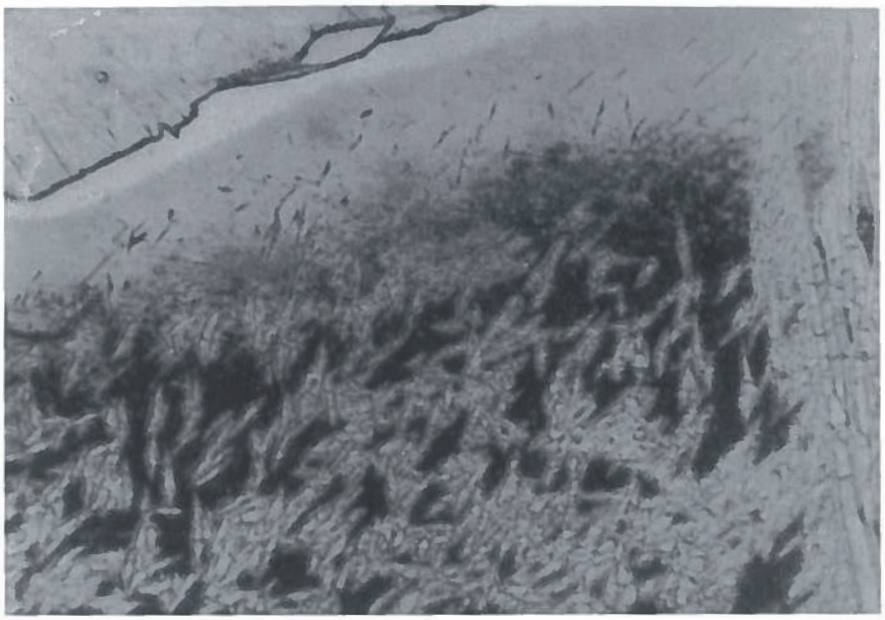

Fig. 11. Martensitic structure in a fine-grained plessite field. Note that the orientation of kamacite needles is not uniform. Etched. Longer side of the photograph equals 0.30 mm.

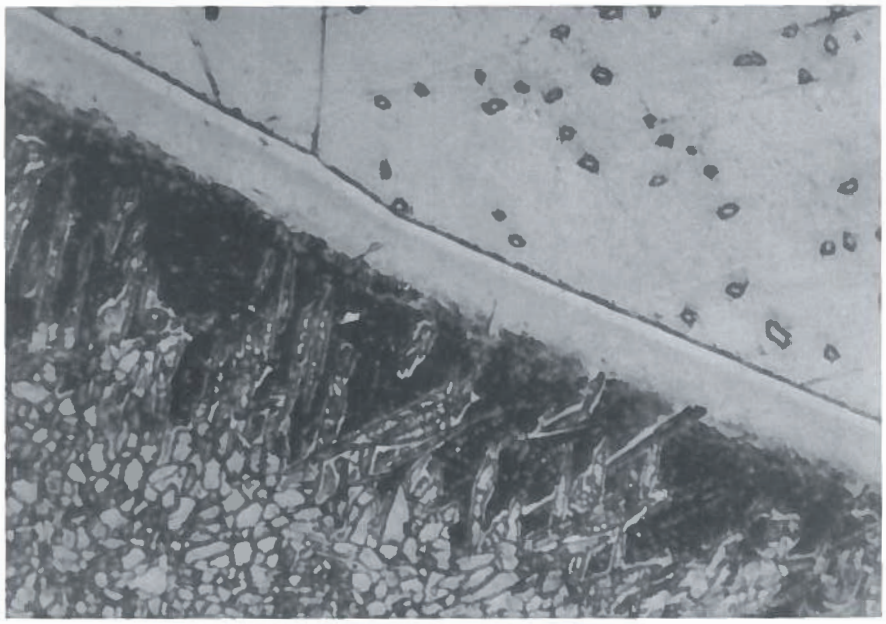

Fig. 12. Zonal development of fine-grained plessite. At the center of the plessitic field, there is a mosaic of kamacite grains, which grades into acicular rim. Further on, these acicular crystals develop into black plessite and taenite. At the contact with a broad kamacite band of the 1st generation taenite contains the highest content of nickel indicated by its white color. Abundant rhabdite crystals dot the kamacite band of the 1st generation. Etched. Longer side of the photograph equals 0.30 mm.

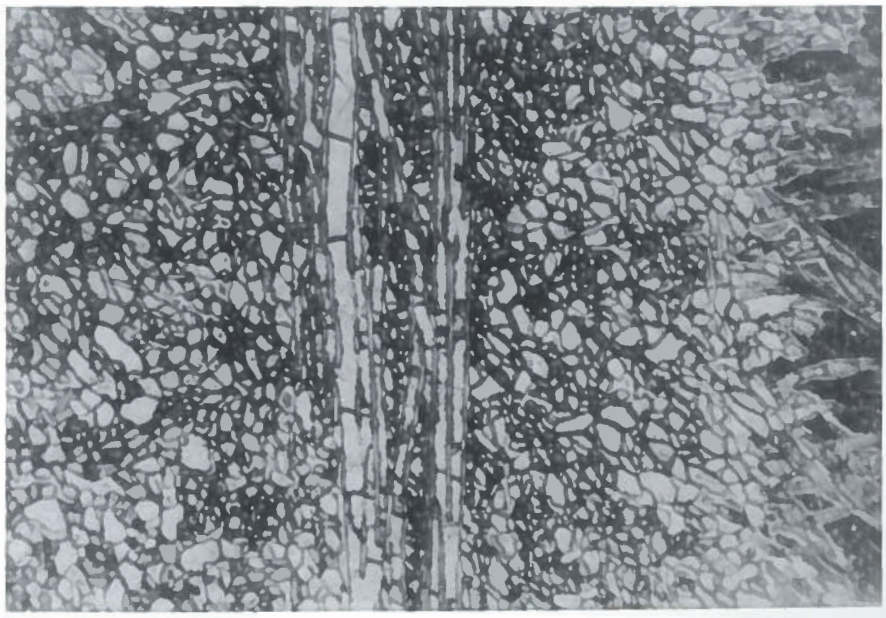

Fig. 13. Typical net plessite revealing two dominant orientations of elongated kamacite grains (light) separated by taenite (black) matrix. Etched. Longer side of the photograph equals 0.30 mm.

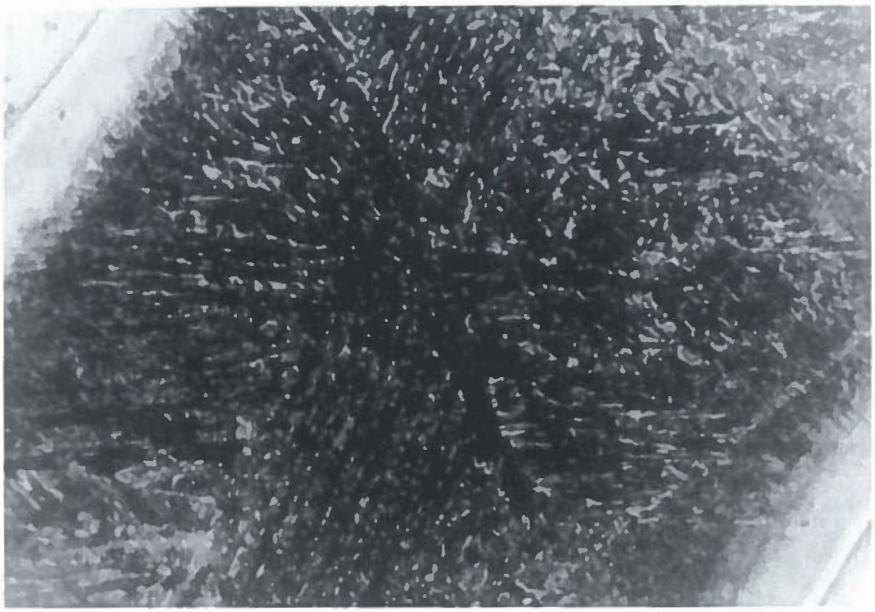

Fig. 14. Black taenite. Kamacite-taenite intergrowths follow the orientation of the Widmanstätten pattern of kamacite bands of the 1st generation. Etched. Longer side of the photograph equals 0.30 mm.

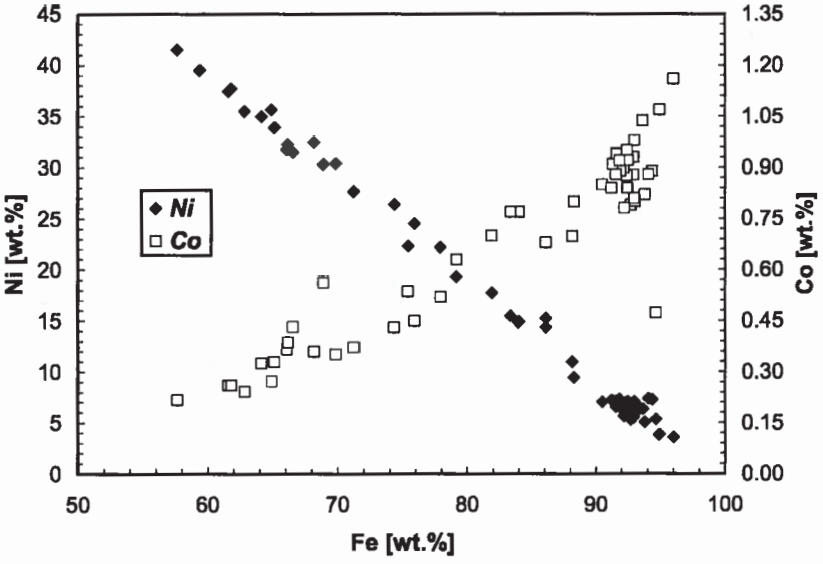

Fig. 15. Plot of Ni and Co contents in wt. % vs. content of Fe in metallic phases. The nickel content is correlated negatively, whereas correlation for Co is positive.

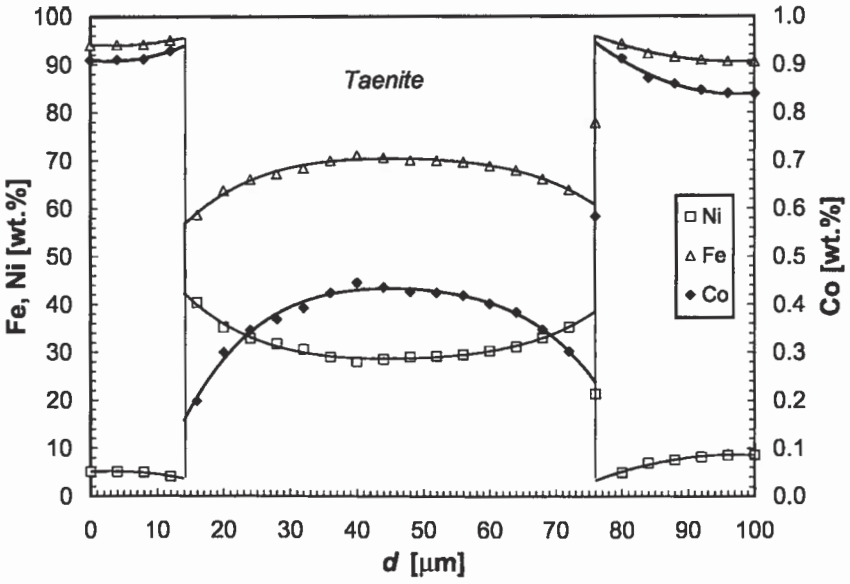

Fig. 16. M-profile traverse through taenite lamella in kamacite. Iron, nickel and cobalt contents in wt. % are shown. Taenite region is about 60 μm wide.

etal, have commonly an irregular lobate outline. Euhedral grains are quite rare. They commonly form complicated elongated or star-shaped skeletal aggregates. These aggregates are usually rimmed by well-developed swathing kamacite up to 2 mm thick, and are a characteristic feature of all sections of the Vicenice octahedrite (Figs 4 and 17). In polished section, schreibersite is anisotropic and yellow with a pink tint close to boundaries with kamacite bands. It is apparently brittle. Skála and Frýda (1996a) refined the crystal structure of schreibersite on material from these skeletal aggregates applying the Rietveld method to X-ray powder diffraction data. Smaller inclusions of schreibersite (~0.1–1.0 mm in diameter) embedded in kamacite plates are also relatively abundant. Kamacite bands widen somewhat around these schreibersite grains. In plessitic fields, tiny grains of schreibersite (up to 0.1 mm) are observed, usually at boundaries of taenite lamellae rims with kamacite bands of the 2nd type. Schreibersite is almost universally encased in kamacite, which forms at least a thin rim around schreibersite at the contact with taenite (Fig. 18). Schreibersite grains are encountered in direct contact with taenite only exceptionally (Fig. 19). Chemical data for larger skeletal schreibersites are given in Table 3.

Besides the described morphological types, schreibersite also forms fringes along some chromite grains in kamacite and veinlets connecting individual larger grains in skeletal aggregates. Both these types have elevated nickel content compared to that of skeletal crystals and aggregates (see Table 4).

Euhedral crystals of schreibersite – so-called rhabdites – are square-, lozenge- or rectangle-shaped depending on

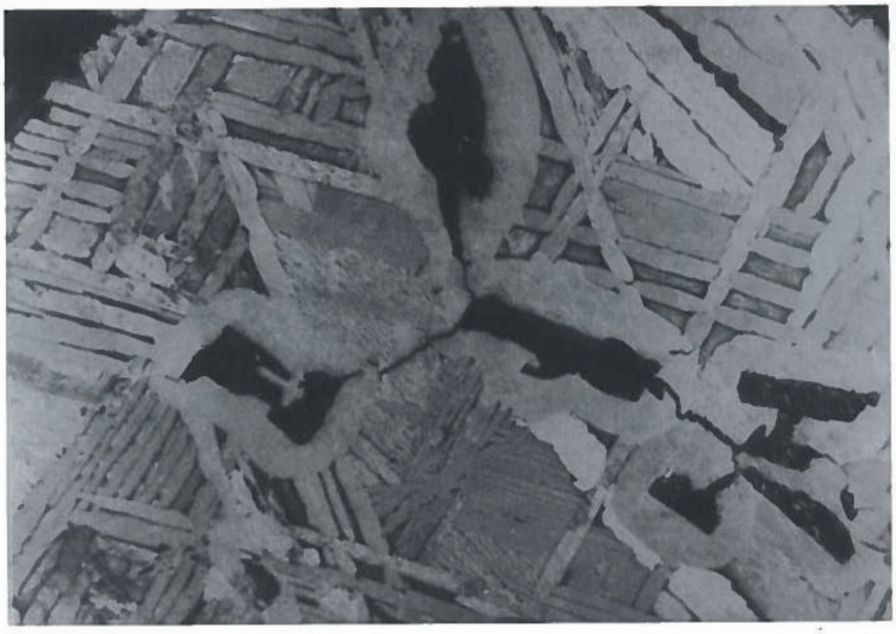

Fig. 17. Skeletal aggregate of schreibersite enveloped by swathing kamacite in the surface 'e'. The Widmanstätten pattern of kamacite bands of the 1st generation and coarse-grained plessites formed by kamacite of the 2nd generation are also shown. Etched. Longer side of the photograph equals 7.5 mm.

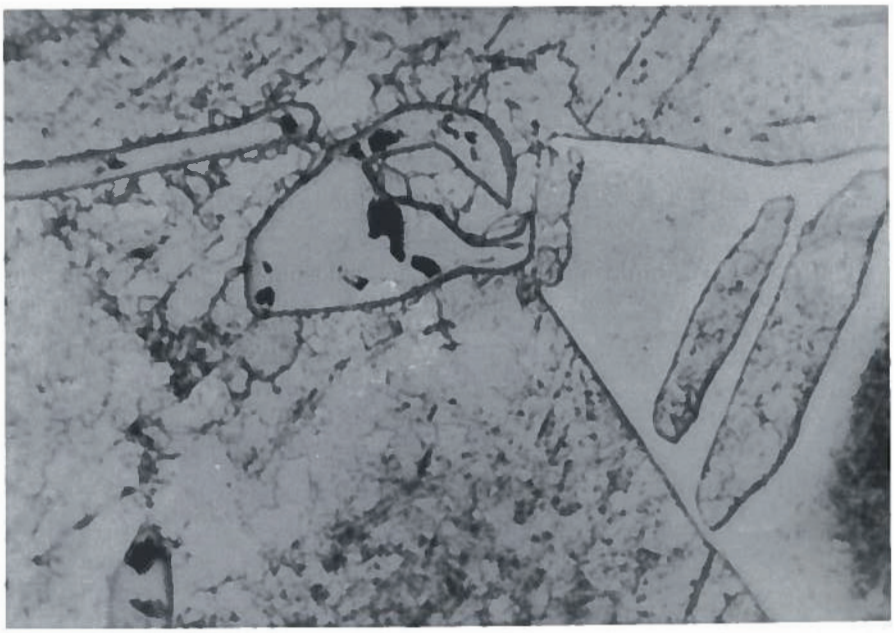

Fig. 18. Two irregular schreibersite grains near the contact with taenite of the plessitic field are enclosed in kamacite, which obviates the direct contact with taenite. This is a quite common texture. Cf. Fig. 19. Etched. Longer side of the photograph equals 0.36 mm.

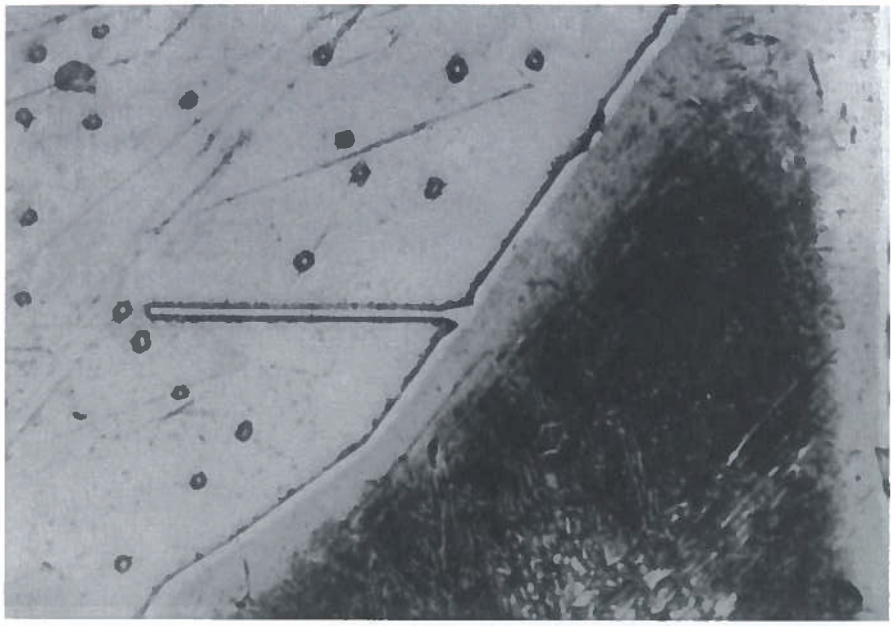

Fig. 19. An extremely rare case of schreibersite (rhabdite) in direct contact with taenite. Note that rhabdites are present in two orientations in the kamacite band of the 1st generation. Whereas most sections seen on the photograph are latitudinal, the crystal in contact with taenite is sectioned longitudinally. Etched. Longer side of the photograph equals 0.36 mm.

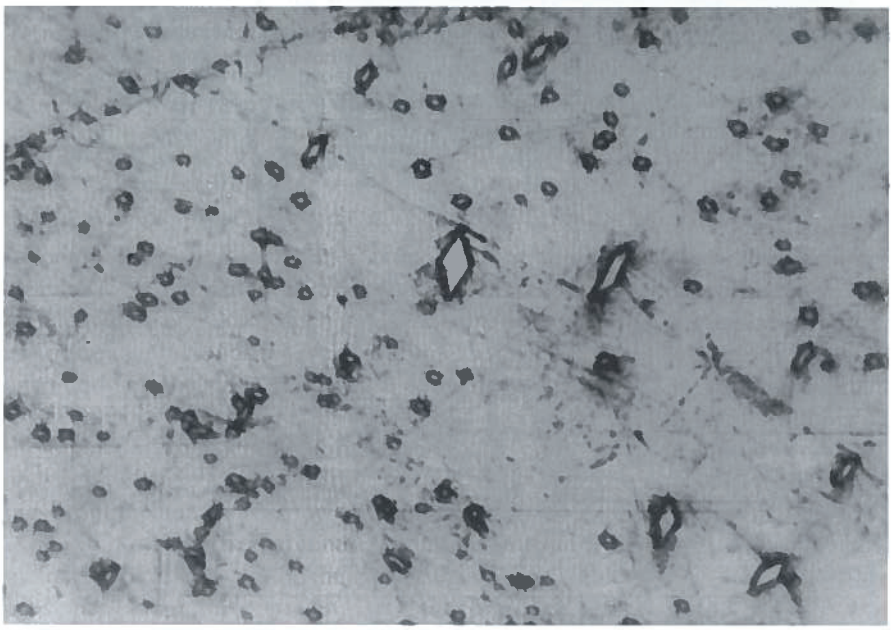

Fig. 20. Schreibersite, variety rhabdite, in the kamacite band of the 1st generation. Etched. Longer side of the photograph equals 0.30 mm.

direction under which they are sectioned (Figs 19–20). Rhabdites are found in kamacite bands of both 1st and 2nd generation. Latitudinal sections through rhabdite crystals reach up to 0.01 mm. In single kamacite grains, rhabdite crystals posses usually a single (and locally two or more) specific crystallographic orientation, suggesting a crystallographic relationship between cubic kamacite and tetragonal schreibersite. This relationship has recently been defined by Hennig et al. (1999) as $\{110\}(FeNi)_3P \parallel \{210\}\ \alpha$-(Fe,Ni) $\cap\ \langle 001\rangle\ (Fe,Ni)_3P \parallel \langle 001\rangle\ \alpha$-(Fe,Ni) by Kossel diffraction using an SEM on samples of Toluca and Morasko iron meteorites. Chemical data for Vicenice rhabdites are summarized in Table 5.

The Vicenice iron contains also a new mineral nickelphoshide – Ni-dominant analog of schreibersite – which has recently been described from the meteorite Butler (Britvin et al. 1999). In the Vicenice meteorite, it has been identified as small – usually 40–80 μm long and 10–20 μm wide – irregular anhedral grains embedded in kamacite. It occurs either in kamacite lamellae near or at the contact with taenite or in plessitic fields. See Fig. 21. Compositional data for this phase are given in Table 6.

Plot in Fig. 22 correlates the chemical composition of schreibersite in the Vicenice octahedrite with various morphological types. Larger grains and skeletal aggregates are characterized by the lowest nickel content, whereas rhabdite crystals have Fe/Ni ratio close to ½. In Ni-dominant analogs of schreibersite, nickel even dominates over iron. Clearly, individual schreibersite types are products of different crystallization processes with varying amount of nickel available to enter crystal structure of a particular schreibersite type.

Table 3. Chemical composition and atoms per formula unit for large schreibersite grains and skeletal aggregates from the Vicenice octahedrite.

	wt. %				apfu	
	Range		Mean	esd	Mean	esd
Fe	59.66	66.11	61.70	1.24	2.216	0.034
Ni	20.96	24.54	22.50	1.01	0.769	0.034
Co	0.08	0.55	0.28	0.08	0.010	0.003
Cr	0.00	0.10	0.03	0.03	0.001	0.001
P	14.67	15.92	15.45	0.21	1.001	0.007
S	0.05	0.17	0.09	0.03	0.003	0.003
Total			100.05	1.62		

Note: Atomic contents were normalized to 4 atoms pfu.

Table 4. Chemical composition and atoms per formula unit for schreibersite in fringes along chromite crystals, and in veinlets connecting individual larger grains in schreibersite skeletal aggregates.

	wt. %				apfu	
	Range		Mean	esd	Mean	esd
Fe	46.82	51.69	49.46	1.29	1.781	0.041
Ni	32.58	37.44	35.02	1.18	1.200	0.043
Co	0.01	0.32	0.17	0.08	0.006	0.003
Cr	0.00	0.29	0.06	0.08	0.002	0.003
P	15.28	15.75	15.50	0.13	1.007	0.004
S	0.03	0.12	0.06	0.03	0.004	0.002
Total			100.27	1.76		

Note: Atomic contents were normalized to 4 atoms pfu.

Table 5. Chemical composition and atoms per formula unit for euhedral schreibersite crystals (rhabdites).

	Analyses in wt. %				Formula in afu	
	Range		Mean	esd	Mean	esd
Fe	41.82	42.06	41.95	0.11	1.521	0.004
Ni	42.48	43.17	42.83	0.29	1.478	0.006
Co	0.05	0.07	0.07	0.01	0.002	0.000
Cr	0.01	0.07	0.03	0.03	0.001	0.001
P	15.18	15.27	15.22	0.04	0.995	0.004
S	0.02	0.07	0.05	0.02	0.003	0.001
Total			100.14	0.31		

Note: Atomic contents were normalized to 4 atoms pfu.

Table 6. Chemical composition and atoms per formula unit for nickelphosphide from the Vicenice octahedrite.

	wt. %				apfu	
	Range		Mean	esd	Mean	esd
Fe	34.84	38.04	35.95	0.70	1.312	0.025
Ni	46.45	50.16	48.57	0.74	1.687	0.024
Co	0.00	0.27	0.12	0.07	0.003	0.003
Cr	0.01	0.09	0.03	0.02	0.001	0.001
P	14.77	15.47	15.12	0.18	0.995	0.008
S	0.01	0.13	0.04	0.03	0.002	0.002
Total			99.83	1.04		

Note: Atomic contents were normalized to 4 atoms pfu.

Troilite

Troilite forms nodules, typically 0.5–1 mm across, or subhedral grains up to 400 × 250 μm. It is relatively rare constituent of the Vicenice iron, encounterd either directly in kamacite or in schreibersite. In polished section, it

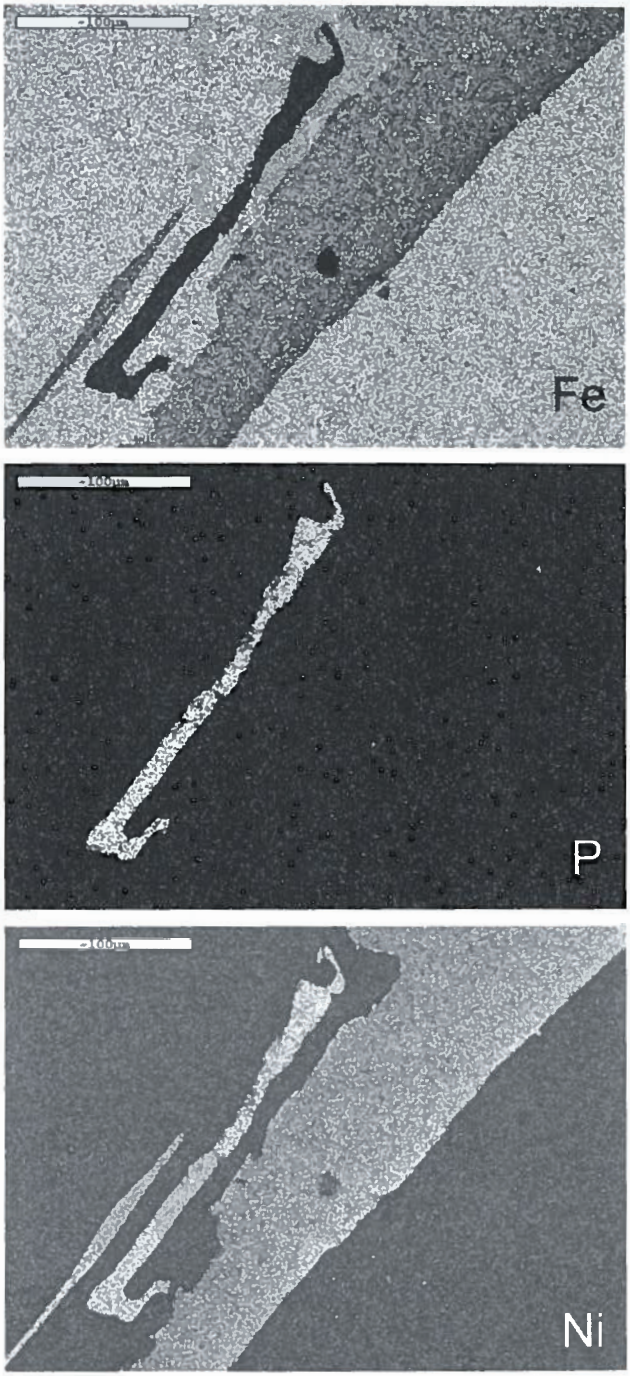

Fig. 21. Unusually long grain of nickelphosphide in a plessite field. Distribution maps for Fe, P and Ni. Scale bar equals 100 μm.

is pale brownish-bronze colored with a greenish tint. This color darkens with time. Troilite is strongly anisotropic. Troilite with significantly elevated Cr content was encountered besides almost pure FeS compositions (Tables 7 and 8). This Cr-rich troilite was observed as a single lamella about 30 μm wide running across a subhedral troilite grain (Fig. 23), and as a portion (~ 250 × 40 μm in size) of another elongated subhedral troilite grain. In both cases, the chromium may have been derived from a reaction with original daubréelite intergrown with troilite (see below).

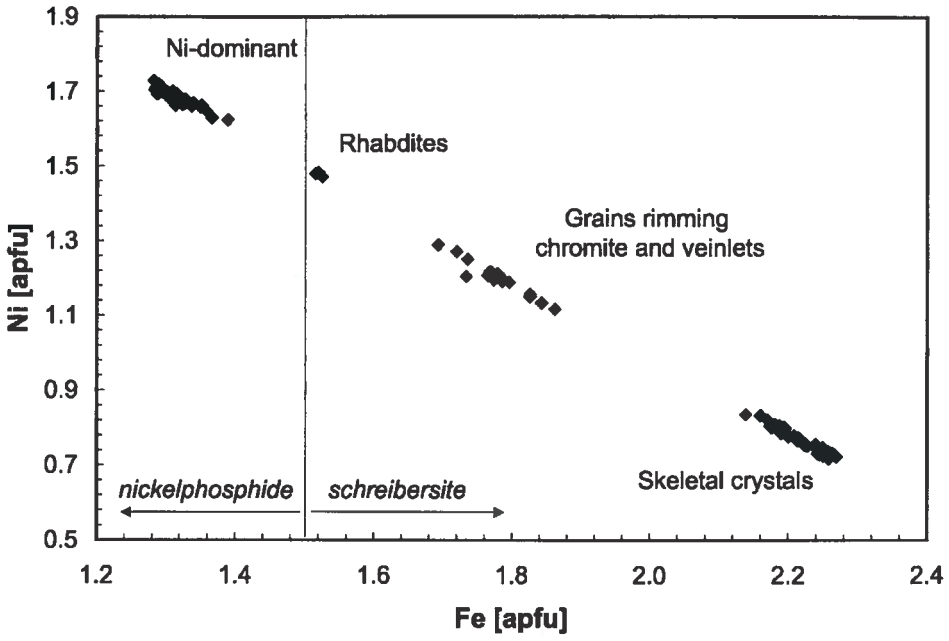

Fig. 22. Plot of Ni vs. Fe contents (apfu) in schreibersites. Four well-defined clusters were observed, which are correlated to morphological appearance. Whereas larger grains in skeletal aggregates contain the least amount of nickel, this element dominates in tiny (up to ca 100 μm), usually elongated or platy grains. This Ni-dominant phase corresponds to a recently described new mineral nickelphosphide (Britvin et al. 1999).

Daubréelite

Daubréelite is even scarcer than troilite. Bluish and isotropic, daubréelite forms subhedral grains up to 150 μm in kamacite bands of 1st generation. Its composition is given in Table 9. Probably, it originally also occurred as exsolution product in trolite in form of lamellae parallel to (0001) observed occasionally in other iron meteorites (Buchwald 1975). However, later processes associated with elevated temperature triggered a reaction of these lamellae with host troilite and produced the Cr-rich troilite described above.

Chromite

Euhedral or subhedral to completely anhedral grains of chromite are bluish in reflected light. They attain dimensions of up to 600 × 400 μm. Chromite crystals quite commonly contain inclusions of other minerals, chiefly kamacite but also schreibersite and troilite. Chromite grains are usually encased in kamacite, commonly separated by schreibersite fringes (Fig. 24). The range of chemical compositions, mean composition and a mean atoms pfu are summarized in Table 10. Zinc enters both of the spinel-structure Cr-rich phases – chromite and daubréelite. Though the amounts of total iron and chromium are almost identical in both minerals, they differ in the content of Zn; chromite contains just about half or so zinc compared to daubréelite, despite the fact that daubréelite grains locally adjoin chromite crystals. Clearly, zinc is preferably partitioned into daubréelite. Compositions of both minerals in terms of Cr/(Cr + Fe) and Zn/(Zn + Fe) ratios are compared in Fig. 25.

Oxygen-chlorine bearing phase

This phase was described as lawrencite ($FeCl_2$) in our preliminary report (Skála and Frýda 1994). Later, we recognized that not only chlorine is present but also a considerable amount of oxygen (Skála and Frýda 1996b). Tentatively, we identified this phase as hibbingite (β-$Fe_2(OH)_3Cl$) though it also could be chlorine-containing akaganéite (β-FeOOH) which was originally described as a weathering product from several Antarctic iron meteorites by Buchwald and Clarke (1989). We did not quantify elements because of poor quality of sur-

Table 7. Chemical composition and atoms per formula unit for troilite from the Vicenice octahedrite.

	wt. %				apfu	
	Range		Mean	esd	Mean	esd
Fe	61.80	64.88	63.04	0.79	0.993	0.014
Ni	0.11	1.03	0.42	0.28	0.006	0.004
Co	0.02	0.87	0.20	0.26	0.003	0.004
Cr	0.22	0.93	0.40	0.19	0.007	0.003
P	0.00	0.08	0.02	0.03	0.001	0.001
S	35.30	36.84	36.11	0.48	0.991	0.010
Total			100.19	1.02		

Note: Atomic contents were normalized to 2 atoms pfu.

Table 8. Chemical composition and atoms per formula unit for chromium-rich troilite from the Vicenice octahedrite.

	wt. %				apfu	
	Range		Mean	esd	Mean	esd
Fe	49.37	52.73	51.29	0.86	0.802	0.012
Ni	0.10	0.99	0.31	0.19	0.005	0.003
Co	0.00	0.17	0.06	0.05	0.001	0.001
Cr	9.55	11.33	10.47	0.52	0.176	0.009
P	0.00	0.00	0.00	0.00	0.000	0.000
S	36.56	38.30	37.28	0.40	1.016	0.005
			99.41	1.10		

Note: Atomic contents were normalized to 2 atoms pfu.

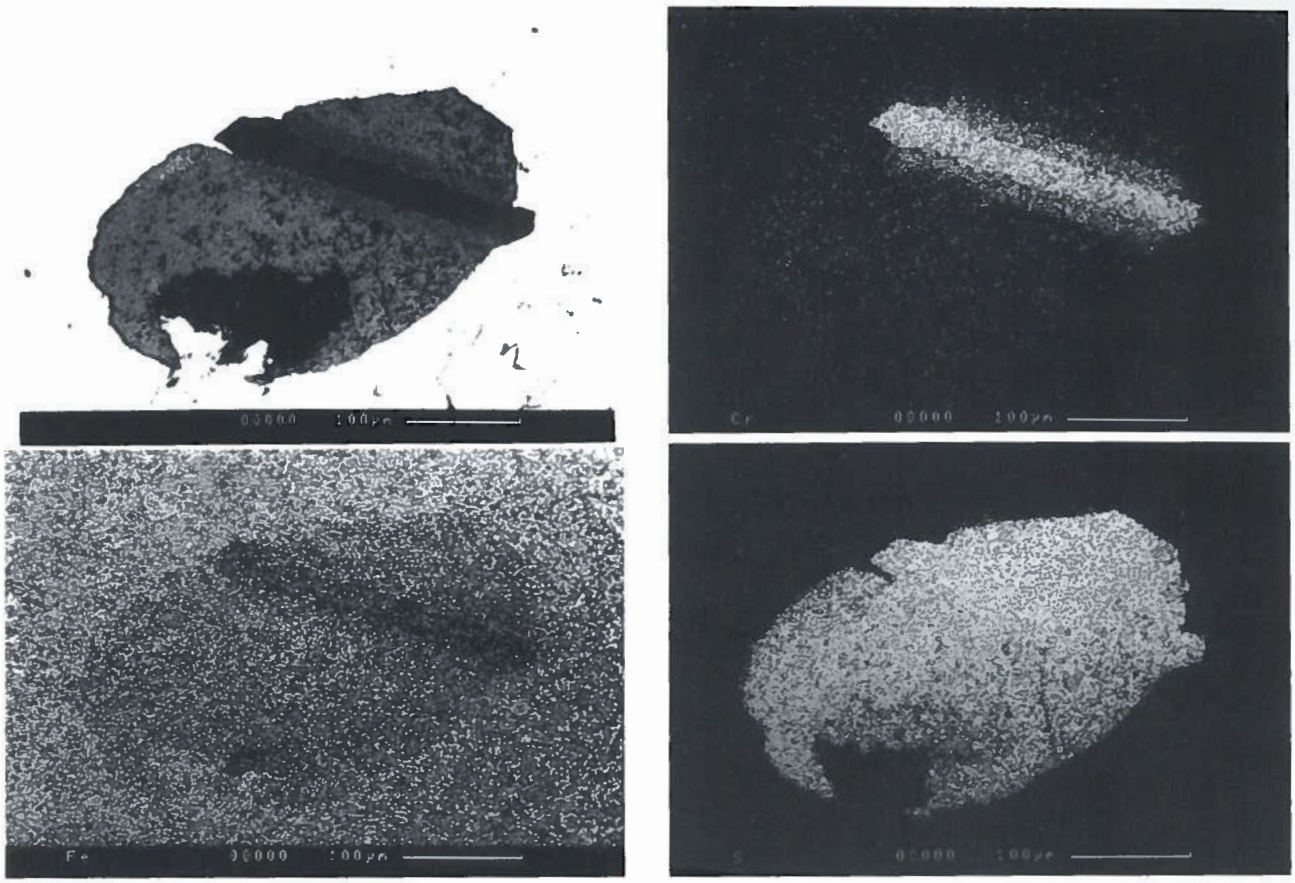

Fig. 23. Subhedral troilite crystal hosting Cr-rich troilite lamella embedded in kamacite. Back-scattered electron image, and distribution maps for Cr, Fe and S are shown. Scale bar equals 100 μm.

face and instability of the phase under the electron beam.

Originally, we found the phase in the form of round inclusion about 30 μm across in one subhedral chromite crystal (600 × 400 μm), associated with inclusions of kamacite, troilite, and schreibersite. Therefore, we speculated about the possibility of primary origin of this phase. However, during detailed search we observed a phase of the same or very similar composition along several cracks and on some grain boundaries. Thus, these observations support a secondary origin of this Fe-O-H-Cl-phase.

Table 9. Chemical composition and atoms per formula unit for daubréelite from the Vicenice octahedrite.

	wt. %				apfu	
	Range		Mean	esd	Mean	esd
Fe	17.31	18.67	17.84	0.41	0.922	0.021
Ni	0.01	0.31	0.13	0.09	0.005	0.005
Co	0.02	0.15	0.08	0.04	0.003	0.003
Cr	35.21	36.91	36.14	0.44	2.005	0.012
Zn	1.32	1.75	1.54	0.14	0.064	0.017
P	0.00	0.17	0.05	0.05	0.005	0.004
S	43.11	45.13	44.41	0.54	3.997	0.019
Total			100.09	0.83		

Note: Atomic contents were normalized to 3 cations pfu.

Space deformation, cooling, and terrestrial weathering

Space deformations

The oldest deformation, which affected the Vicenice iron meteorite, is the uniaxial strain (most probably due to a shock) applied to the meteorite probably before the Widmanstätten pattern had formed, i. e. at the time when the meteorite consisted of a single grain of the γ-phase. This deformation of the γ-phase resulted in distortion of 3D geometry of the subsequently formed kamacite bands.

However, there are even more prominent features indicating strong mechanical shock-induced deformation, which affected the meteorite below the $\gamma/(\gamma+\alpha)$ phase boundary. These are various localized rupture zones. Kamacite bands, taenite lamellae and plessite fields are quite commonly broken and displaced (Figs 26–28) or plastically deformed (Fig. 29); occasionally, this type of deformation results in granulation of the only kamacite bands (Figs 30–31).

Other mechanically induced deformations include the Neumann bands in kamacite plates. They are observed in the Vicenice iron chiefly in smaller kamacite grains at or near fine-granulated rupture zones (Fig. 32); if in larger kamacite grains, they are developed in places where elevated strain rates could be expected. They are quite commonly encountered at the contact of kamacite

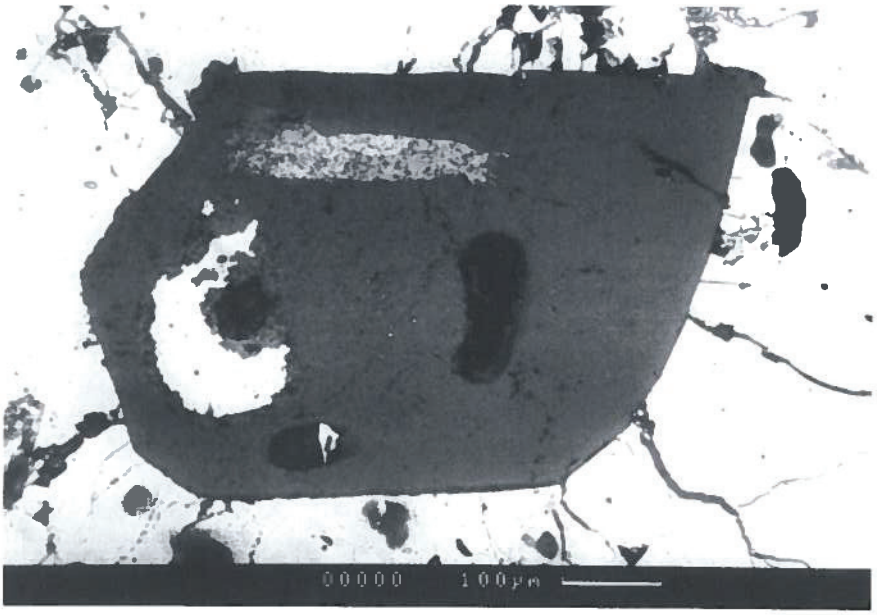

Fig. 24. Back-scattered electron image of subhedral grain of chromite containing inclusions of kamacite, schreibersite, troilite and oxygen-chlorine bearing iron (hydro?)oxide. Scale bar equals 100 μm.

Table 10. Chemical composition and atoms per formula unit for chromite from the Vicenice octahedrite.

	wt. %				apfu		
	Range		Mean	esd		Mean	esd
SiO_2	0.08	0.30	0.18	0.06	Si	0.004	0.004
TiO_2	0.00	0.14	0.02	0.04	Ti	0.001	0.001
Cr_2O_3	67.03	69.11	68.00	0.49	Cr	2.010	0.010
Al_2O_3	0.00	0.17	0.06	0.05	Al	0.002	0.002
FeO^{tot}	28.96	30.20	29.61	0.31	Fe^{3+}	0.010	0.005
					Fe^{2+}	0.915	0.011
MgO	0.00	0.33	0.06	0.07	Mg	0.003	0.004
MnO	0.28	1.21	0.76	0.19	Mn	0.024	0.006
NiO	0.00	0.21	0.06	0.07	Ni	0.002	0.006
ZnO	0.47	1.56	1.03	0.26	Zn	0.028	0.007
Total			99.79	0.68			
					Fe^{tot}	0.926	0.008

Note: Atomic contents were normalized to 3 cations and 4 oxygens pfu.

with minerals of different mechanical properties, such as larger inclusions of troilite or schreibersite. In such cases heavily brecciated rims developed with abundant Neumann bands. It is also noteworthy that three orientations of the Neumann bands are the maximum observed. Locally, bands of one orientation displace those of another one, indicating either complex strain-stress conditions during a single-shock event, or multiple collisions in space (Figs 33–34).

Another cosmic event, characterized by elevated uniaxial pressure associated with temperature increase, produced mosaic structure in some kamacite bands and portions of swathing kamacite. The temperature during this event, however, did not exceed the boundary $\gamma/(\gamma+\alpha)$ in the Fe-Ni binary phase diagram, which corresponds approximately to 700 °C for the Ni content of about

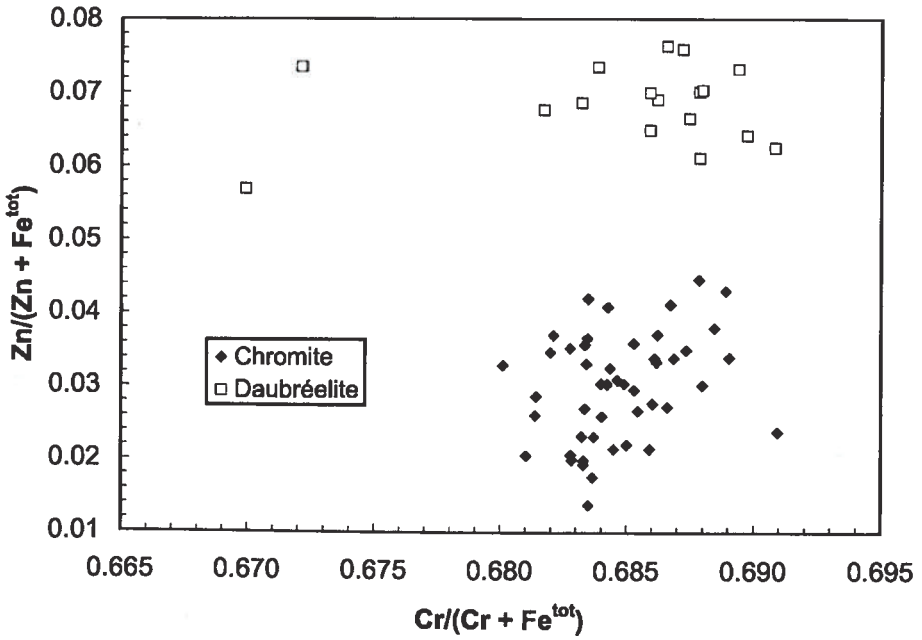

Fig. 25. Comparison of contents of Zn, Cr and Fe^{tot} in spinel-structure phases – chromite and daubréelite. Whereas chromium and total iron contents are more or less identical, the content of zinc in daubréelite is about twice of that measured in chromite.

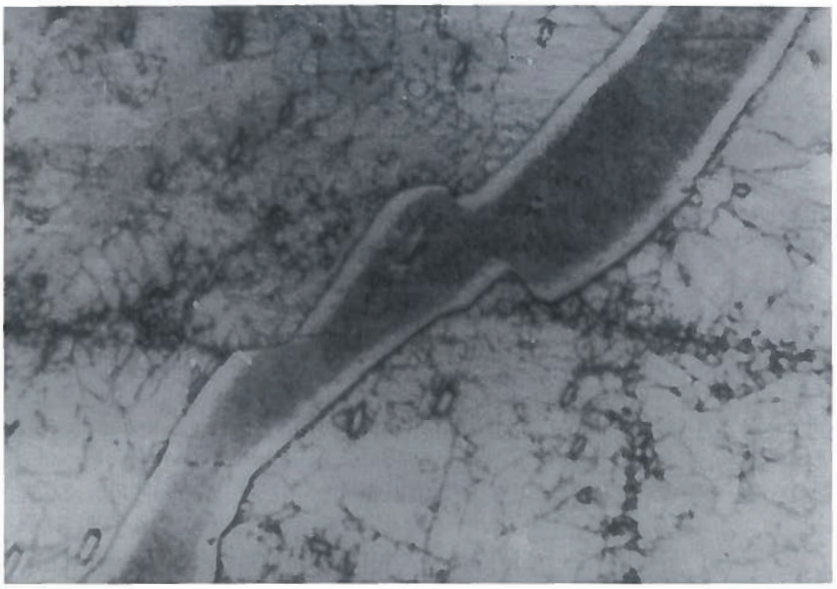

Fig. 26. Dislocation of taenite lamella between two kamacite bands of the 1st generation. Note characteristic zoning of taenite enriched in nickel along contacts with kamacite, and granulation of kamacite along a shear zone down to which the taenite lamella is displaced. Etched. Longer side of the photograph equals 0.36 mm.

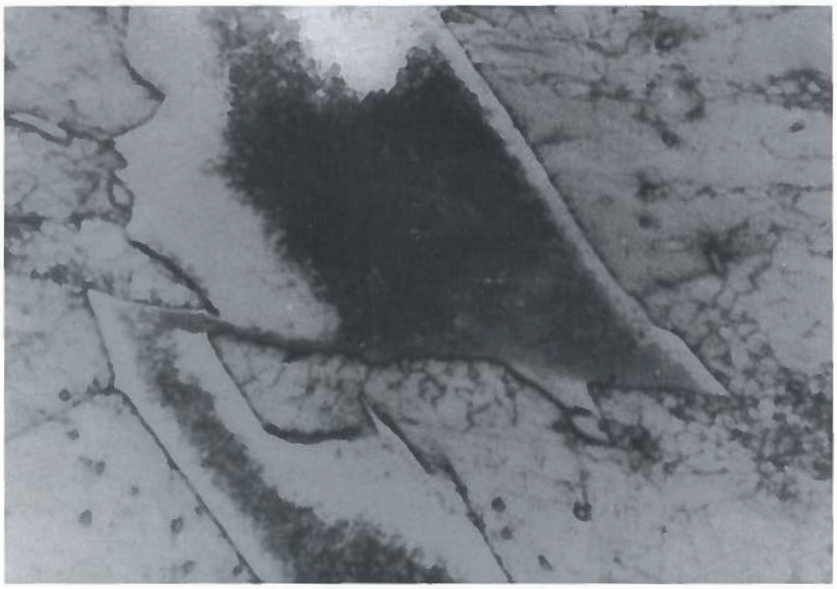

Fig. 27. Displaced field of black plessite. Granulation of kamacite decorates the shear zone, along which the plessite field is displaced. Etched. Longer side of the photograph equals 0.36 mm.

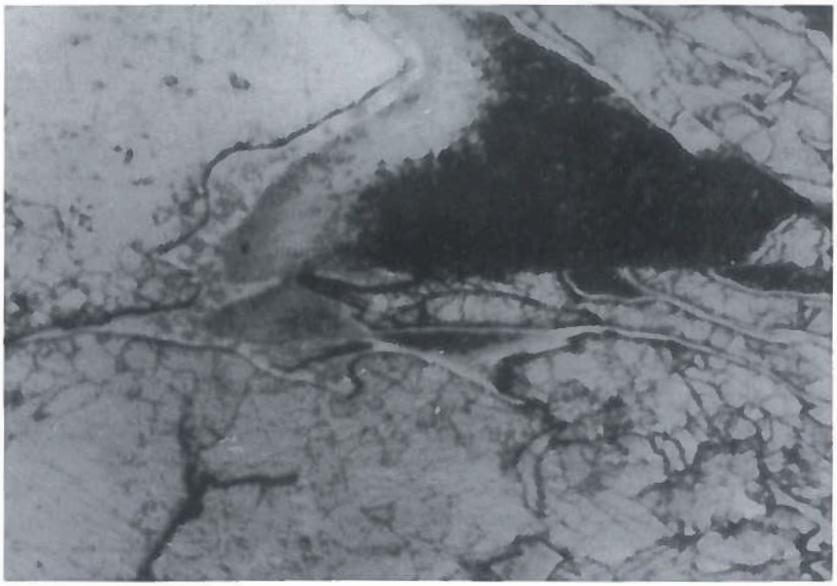

Fig. 28. Complicated deformation of black taenite field and adjacent kamacite bands. Etched. Longer side of the photograph equals 0.36 mm.

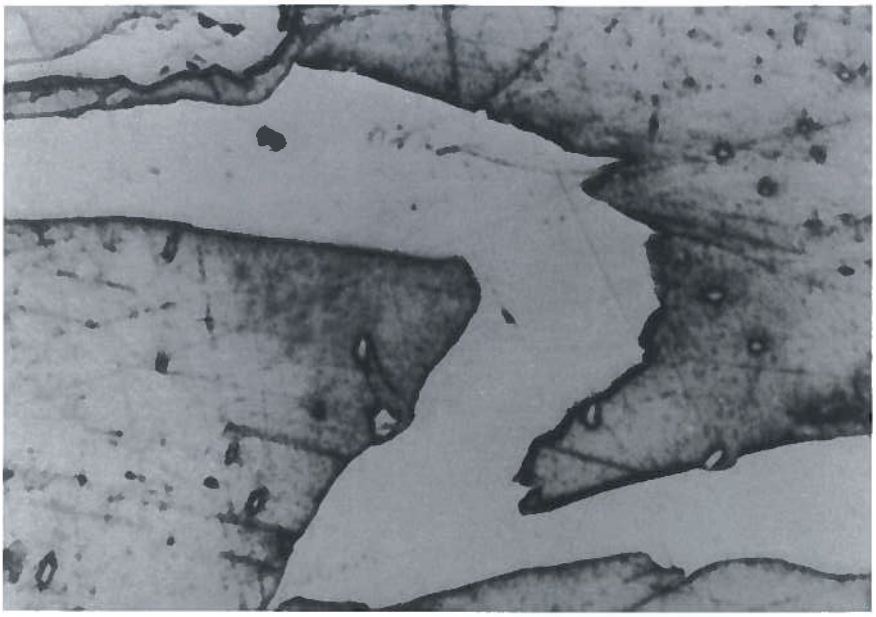

Fig. 29. Plastic deformation of narrow taenite lamella. Etched. Longer side of the photograph equals 0.30 mm.

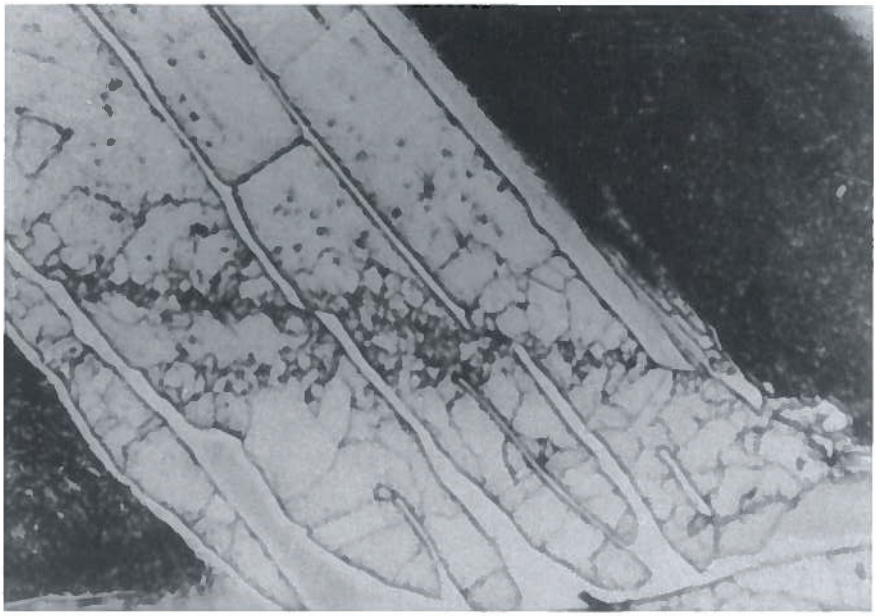

Fig. 30. Rupture sectioning the comb plessite associated with granulation of kamacite bands of the 2nd generation. Etched. Longer side of the photograph equals 0.36 mm.

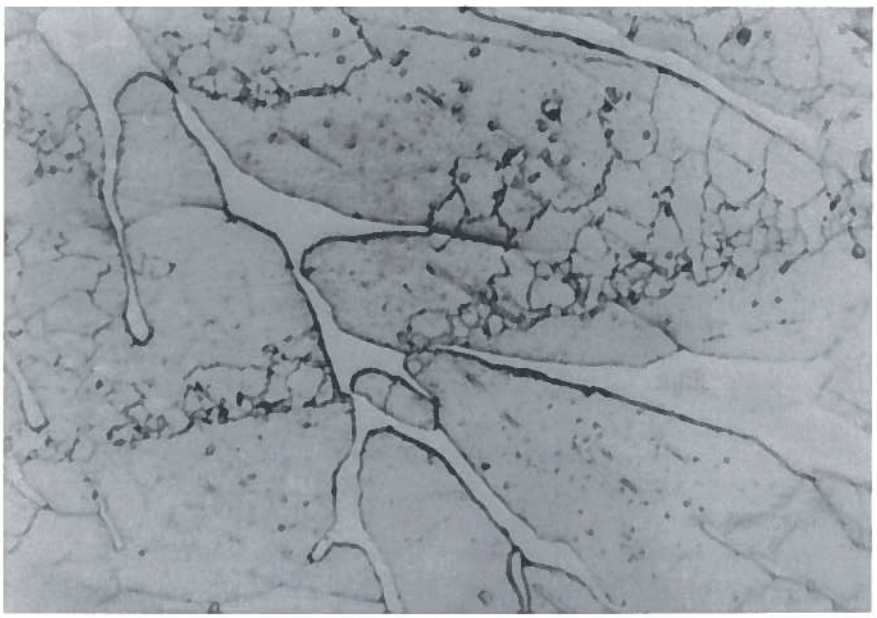

Fig. 31. Typical development of granulation associated with deformation of kamacite bands of the 2nd generation in the comb plessite. Etched. Longer side of the photograph equals 0.36 mm.

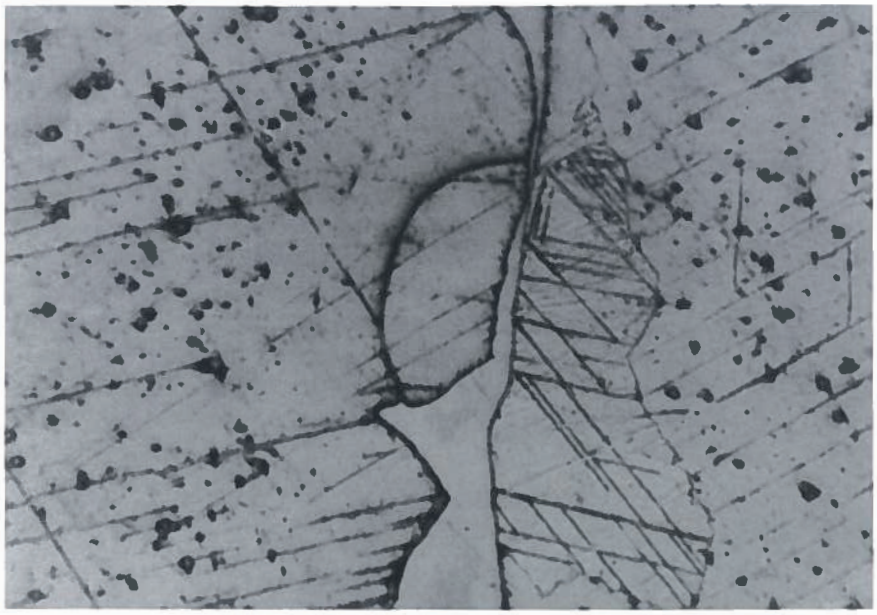

Fig. 32. The Neumann bands are more frequently encountered in the smaller kamacite grains. Etched. Longer side of the photograph equals 0.36 mm.

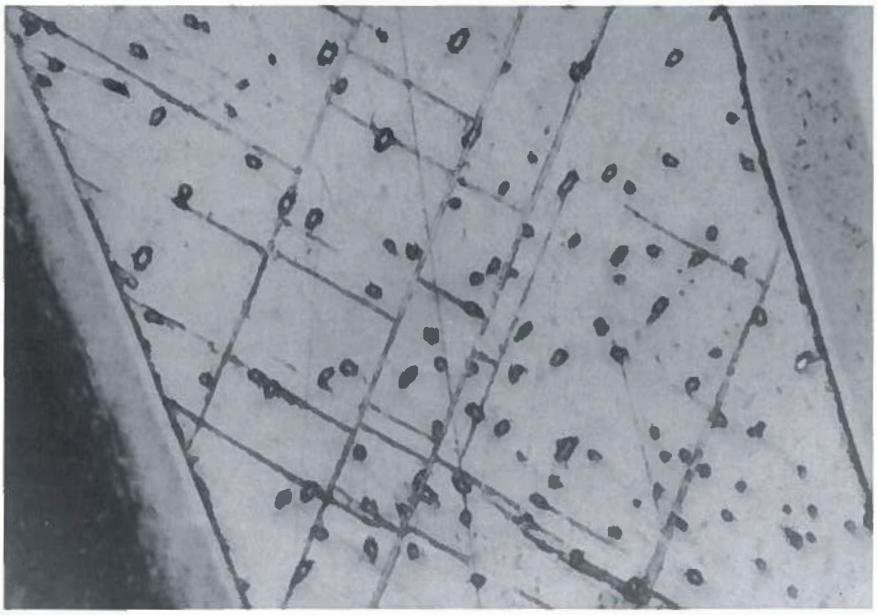

Fig. 33. Kamacite band with rhabdite crystals and a ladder-shaped net of the Neumann bands displacing each other. Two orientations of the Neumann bands are encountered. Etched. Longer side of the photograph equals 0.36 mm.

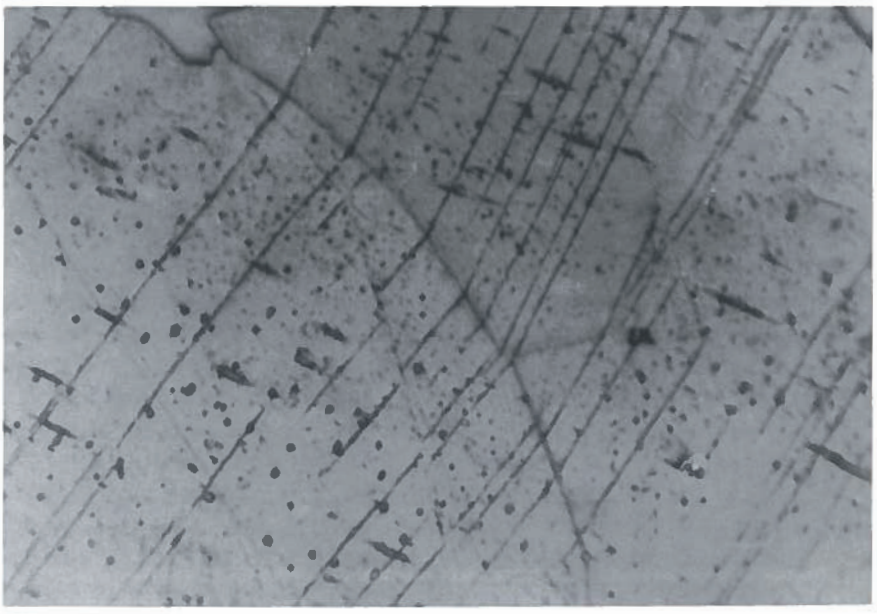

Fig. 34. The Neumann bands broken at the contact of two kamacite grains. Note also abundant rhabdite crystals in the kamacite grains. Etched. Longer side of the photograph equals 0.36 mm.

9.7 wt. % (Kaufman – Cohen 1956; Goldstein – Ogilvie 1965).

A heat-affected zone, formed during atmospheric entry and fall, is developed in the Vicenice octahedrite as a layer up to 12 mm thick in the cut surface 'f' (Fig. 3), but considerably narrower in surface 'a' (Fig. 5). The so-called α_2 zone with characteristic matte appearance is only 1 mm thick in all sections.

Cooling rate

Despite of uncertainties associated with calculations of cooling rates (Buchwald 1975) we have applied the simplified Short and Goldstein's (1967) approach to estimate the cooling rate for the Vicenice octahedrite. Based on the bulk content of nickel which is 9.7–9.8 wt. % and the kamacite bandwidth (0.63 mm) the cooling rate is about 1.5–2 °C/Ma. The formula of Wasson (1971) yielded similar values – 1.8 to 1.9 °C/Ma‡.

Terrestrial weathering

As already noted above, the meteorite has been recovered from a loamy soil from a depth of about 0.75 m. It was covered with 6–8 mm thick weathering crust. Originally, this crust was continuous, probably covering the whole surface of the meteorite, and it was composed of two individual layers. The inner, more compact, thinner, more or less well preserved layer occurred directly in the contact with metal, into which it penetrated in some places to the depth of up to several millimeters. This layer apparently originated at the expense of the meteorite during its weathering in the soil horizon. On the contrary, the outer, thicker, ochre-colored layer easily crumbled and was generated by deposition of iron oxide-hydroxides from the adjacent loamy soil.

X-ray powder diffraction on material taken from one of small depressions on the meteorite surface proved the presence of goethite (α-FeOOH) and lepidocrocite (γ-FeOOH) in the inner layer of the meteorite weathering crust. Also, admixtures of quartz and K-feldspar were identified in this crust representing apparently contaminants from the soil.

‡ Depending on Ni content taken into an account during the calculation.

Acknowledgements. Authors are grateful to the National Museum in Prague for the loan of a slice of the Vicenice iron meteorite. The constructive and careful review by Marcela Bukovanská is gratefully acknowledged. The research has been supported by the grant project No. 205/98/0655 from the Grant Agency of the Czech Republic.

Submitted January 28, 2000

References

Britvin, S. N. – Kolomensky, V. D. – Boldyreva, M. M. – Bogdanova, A. N. – Kretser, Yu. L. – Boldyreva, O. N. – Rudashevsky, N. S. (1999): Nickelphosphide $(Ni,Fe)_3P$ – the nickel analog of schreibersite. – Zapiski Vseros. Mineral. Obsch., 3, 64–72.

Buchwald, V. F. (1969): Iron meteorites: Tables relating the Widmanstätten angles to the plane of section. – Geochim. Cosmochim. Acta, 33, 152–153.

Buchwald, V. F. (1975): Handbook of Iron Meteorites. Vol. 1. Iron Meteorites in General. – University of California Press, Berkeley, vii + 243 pp.

Buchwald, V. F. – Clarke, R. S. Jr. (1989): Corrosion of Fe-Ni alloys by Cl-containing akaganéite (β-FeOOH): The Antarctic meteorite case. – Amer. Mineral., 74, 656–667.

Goldstein, J. I. – Ogilvie, R. E. (1965): A re-evaluation of the iron-rich portion of Fe-Ni system. – Transactions of the Metallurgical Society, American Institute of Mining and Metallurgical Engineers 233, 2083–2087.

Hennig, C. – Geist, V. – Heide, G. (1999): Investigation of the rhabdite/kamacite law of intergrowth in iron meteorites with the aid of the Kossel technique. – Meteoritics and Planet. Sci., 34, 61–66.

Kaufman, L. – Cohen, M. (1956): The martensitic transformation in the iron-nickel system. – Transaction AIME, Journal of Metals, 208, 1393–1401.

Sekanina, J. (1971a): Železný meteorit (oktaedrit) Vícenice u Náměště n. Oslavou. – unpublished report (81 pp.) and photo-atlas (158 figs), Brno. (In Czech).

Sekanina, J. (1971b): Kosmická mineralogie. – Folia. Fac. Sci. Nat. Univ. Purkynianea Brunensis 12, Geologica 21, 6, 63–76.

Short, J. M. – Goldstein, J. I. (1967): Rapid methods of determining cooling rates of iron and stony iron meteorites. – Science, 156, 59–61.

Skála, R. – Frýda, J. (1994): Mineralogy of the Vicenice iron meteorite. – Meteoritics, 29 (4), 534–535 (abstract).

Skála, R. – Frýda, J. (1996a): Schreibersite from the Vicenice iron: Rietveld crystal structure refinement – A preliminary report. Lunar Planet. Sci. XXVII, 1211–1212, LPI, Houston.

Skála, R. – Frýda, J. (1996b): Primary chlorine-bearing inclusion in meteoritic iron? – Meteoritics and Planet. Sci., 31 (Supplement), A 131 (abstract).

Wasson, J. T. (1971): An equation for the determination of iron-meteorite cooling rates. – Meteoritics, 6, 139–147.

Wasson, J. T. – Ouyang, X. – Wang, J. – Jerde, E. (1989): Chemical classification of iron meteorites: XI Multi-element studies of 38 new irons and the high abundance of ungrouped irons from Antarctica. – Geochim. Cosmochim. Acta, 53, 735–744.

Mineralogie vícenického oktaedritu

Železný meteorit Vicenice byl nalezen v říjnu roku 1911 východně od obce Vícenice u Náměšti nad Oslavou. Jeho původní rozměry byly 180 × 90 × 65 mm a hmotnost 4650 g. Na základě šířky kamacitových pásků se železný meteorit Vicenice řadí do skupiny středních oktaedritů (Om). Chemicky tento meteorit patří mezi železa skupiny IID. Kromě kamacitu a ténitu meteorit obsahuje schreibersit, troilit, daubréelit, chromit a blíže neidentifikovatelný chlór obsahující (hydro?)oxid železa. Schreibersit se ve vicenickém železném meteoritu vyskytuje jako několik různých generací, odlišujících se morfologií a chemismem. Jedna z těchto generací přitom představuje Ni-dominantní fázi, která byla v současnosti popsána jako nový minerál niklfosfid. Několik zrn troilitu obsahue značně zvýšený obsah chrómu. Optická pozorování ukazují, že meteorit byl postižen několika deformacemi, vyvolanými šokovou metamorfózou během kolizí ve vesmíru. Rychlost chladnutí byla pro vícenický meteorit na základě chemismu a šířky kamacitových lišt stanovena v řádu 1.5–2 °C/Ma. Jako hlavní korozní produkty ve zvětrávací kůře pokrývající meteorit byly určeny práškovou rtg. difrakcí goethit a lepidokrokit.